Water Splitting Hot Paper

DOI: 10.1002/anie.201411494

Intercalation of Highly Dispersed Metal Nanoclusters into a Layered Metal Oxide for Photocatalytic Overall Water Splitting**

*Takayoshi Oshima, Daling Lu, Osamu Ishitani, and Kazuhiko Maeda**

Abstract: *Metal nanoclusters (involving metals such as platinum) with a diameter smaller than 1 nm were deposited on the interlayer nanospace of $KCa_2Nb_3O_{10}$ using the electrostatic attraction between a cationic metal complex (e.g., $[Pt(NH_3)_4]Cl_2$) and a negatively charged two-dimensional $Ca_2Nb_3O_{10}^-$ sheet, without the aid of any additional reagent. The material obtained possessed eight-fold greater photocatalytic activity for water splitting into H_2 and O_2 under band-gap irradiation than the previously reported analog using a RuO_2 promoter. This study highlighted the superior functionality of Pt nanoclusters with diameters smaller than 1 nm for photocatalytic overall water splitting. This material shows the greatest efficiency among nanosheet-based photocatalysts reported to date.*

Nanosized particles are of interest because of their wide range of potential applications,[1] including water-splitting photocatalysis that is a simple form of artificial photosynthesis. Noble-metal nanoparticles, called co-catalysts, dispersed on a semiconductor can improve charge separation and thereby increase photocatalytic activity.[2] Because improvement of activity is usually dependent on the uniformity of the co-catalyst dispersion,[2b] a method that improves the dispersion of noble-metal nanoparticles is highly desirable for improving photocatalytic activity.[3,4]

Certain lamellar metal oxides undergo exfoliation by reaction with a suitable guest molecule, producing unilamellar colloids.[5] The colloids are two-dimensional nanocrystals, also called nanosheets, which consist of 1–2 nm thick metal-oxide layers with lateral dimensions ranging from several hundred nanometers to a few micrometers. The anisotropic feature of nanosheets is potentially useful for applications including cosmetics,[6] electronics,[7] catalysis,[8] and photocatalysis.[9–15] For photocatalytic applications, metal-oxide nanosheets that consist of Ti^{4+} or Nb^{5+} have the ability to reduce and oxidize water under band-gap irradiation.[10,12] Water splitting is achieved when photogenerated electrons and holes migrate to the surface without recombination, reducing and oxidizing surface-adsorbed species.[2b] The nanoscale thickness of the sheets allows for prompt migration of the photogenerated charge carriers to the surface, which contributes to high photocatalytic activity.[9–15] However, an efficient overall water splitting system based on nanosheets has not been reported.

The interlayer nanospace of a lamellar solid is a potential reaction site that possesses unusually high catalytic activity.[8c,16] Therefore, introducing catalytic nanoparticles into the interlayer nanospace is challenging. In a report on heterogeneous photocatalysis, Ebina et al. claimed that RuO_2-intercalated $KCa_2Nb_3O_{10}$ could be prepared by reaction of $Ca_2Nb_3O_{10}^-$ colloidal sheets with ruthenium red, followed by flocculation with KOH and calcination in air.[10b] However, no information was provided about the dispersion of RuO_2 in the interlayer space. Mallouk et al. succeeded in intercalating Au nanoparticles into layered solids such as fluoromica and $HCa_2Nb_3O_{10}$ through pre-intercalation of polyamines with little aggregation.[17] However, this system had limitations, such as the difficulty of completely removing the residual amine species from the interlayer space, and the lack of direct bonding between the intercalated Au and the solid surface. Mallouk and co-workers also reported another system involving highly dispersed $Rh(OH)_3$ nanoparticles intercalated into the interlayer of $KCa_2Nb_3O_{10}$ using covalent interactions via Rh-O-Nb bonds.[13a] Although after calcination $Rh_2O_3/KCa_2Nb_3O_{10}$ exhibited a higher photocatalytic activity for H_2 evolution from an aqueous methanol solution than an analog externally decollated with Pt, the overall water splitting was not successful and the applicability of other metals was not discussed.

This report describes a simple method for intercalating metal nanoclusters into $KCa_2Nb_3O_{10}$ through electrostatic attractions between a cationic metal precursor and a negatively charged $Ca_2Nb_3O_{10}^-$ nanosheet without the use of any additional reagent. The resulting material, exemplified by Pt-intercalated $KCa_2Nb_3O_{10}$ nanosheet aggregates, exhibited activity for water splitting into H_2 and O_2 that was about eight-fold greater than that of a previously reported RuO_2 material.[10b] This is the highest value among nanosheet-based photocatalysts reported for overall water splitting.

Unilamellar colloidal nanosheets of $Ca_2Nb_3O_{10}^-$ stabilized by tetra(*n*-butyl)ammonium (TBA^+) cations were prepared

[*] T. Oshima, Prof. Dr. O. Ishitani, Prof. Dr. K. Maeda
Department of Chemistry
Graduate School of Science and Engineering
Tokyo Institute of Technology
2-12-1-NE-2 Ookayama, Meguro-ku, Tokyo 152-8550 (Japan)
E-mail: maedak@chem.titech.ac.jp
Dr. D. Lu
Center for Advanced Materials Analysis
Tokyo Institute of Technology
2-12-1 Ookayama, Meguro-ku, Tokyo 152-8550 (Japan)

[**] We would like to thank Dr. Naoyuki Hatakeyama (Tokyo Institute of Technology) for assistance in TEM observations. This work was supported by the ENEOS Hydrogen Trust Fund and a Grant-in-Aid for Scientific Research on Innovative Areas (project number 25107512; AnApple). Thanks are also extended to the PRESTO/JST program "Chemical Conversion of Light Energy" and a Grant-in-Aid for Young Scientists (A) (project number 25709078).

Supporting information for this article is available on the WWW under http://dx.doi.org/10.1002/anie.201411494.

according to a previously described method, with some modifications.[10] Details of the preparation of metal-intercalated $KCa_2Nb_3O_{10}$ is included in the Supporting Information. For Pt, an aqueous solution containing a cationic Pt complex, $[Pt(NH_3)_4]Cl_2{\cdot}H_2O$, was added into the nanosheet suspension, followed by stirring for 24 h to allow for adsorption of the cationic complex onto the negatively charged surface of the nanosheets. This method is referred to as the adsorption method, and the preparation scheme is depicted in Scheme 1. For comparison, an anionic complex of $H_2[PtCl_6]{\cdot}6H_2O$ also was employed. Then, KOH was added to precipitate the colloidal nanosheets, followed by drying in an oven at 343 K overnight and heating under a H_2 stream (20 mL min^{-1}) at 473 K to reduce cationic Pt species in the Pt metal. Details of the preparation procedure can be found in the Supporting Information. Fourier transform infrared (FTIR) spectra did not contain a peak assignable to C–H stretching bonds from residual TBAOH.[14e] The specific surface area of the prepared material was about 30 m^2 g^{-1}, close to the values of similar analogs.[10,14b,e] Using a conventional method, Pt was loaded by impregnation with KOH-treated restacked $Ca_2Nb_3O_{10}^-$ sheets and $[Pt(NH_3)_4]Cl_2{\cdot}H_2O$, followed by thermal H_2 treatment.

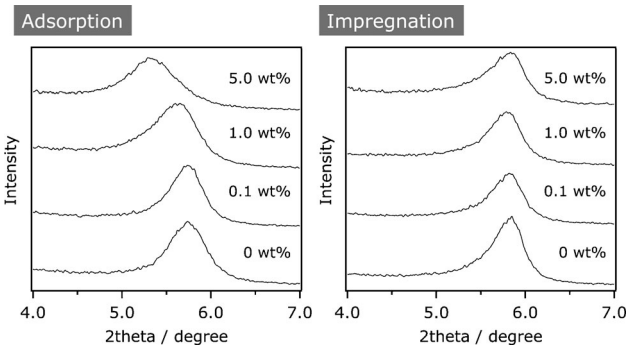

Figure 1. XRD patterns of restacked $KCa_2Nb_3O_{10}$ nanosheets modified with varying amounts of Pt by an adsorption and impregnation method.

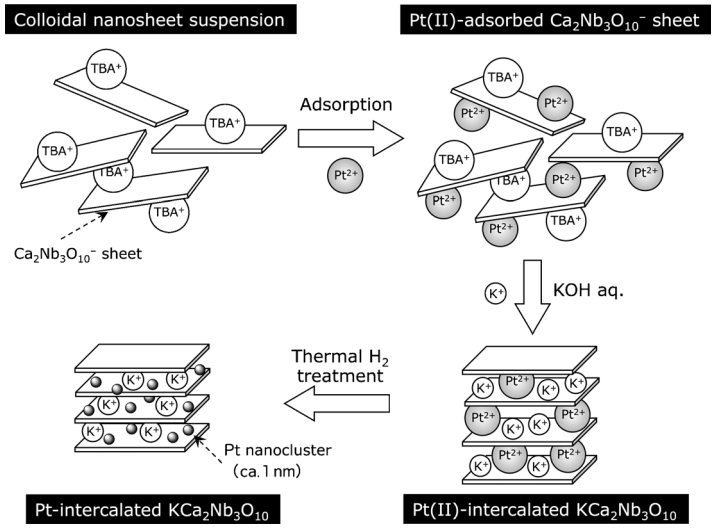

Scheme 1. Preparation of Pt-intercalated $KCa_2Nb_3O_{10}$ nanosheets through electrostatic attraction between a cationic complex and anionic nanosheets [TBA^+ indicates tetra(*n*-butyl)ammonium cation].

Figure 1 shows the XRD patterns of restacked $KCa_2Nb_3O_{10}$ nanosheets prepared by different methods with and without Pt deposition. In the adsorption sample, the (002) diffraction peak appearing at 2θ of about 5.8°, which corresponds to the interlayer spacing of the restacked sheets, shifted to lower angles upon an increase in Pt loading amount. These results indicate the occurrence of interlayer expansion, likely due to intercalation of Pt nanoparticles into the layer nanospace, although another Pt species was located on the external surface of the restacked nanosheets. The *d*-spacings of $KCa_2Nb_3O_{10}$ loaded with 0.1, 1.0, and 5.0 wt% Pt were calculated to be 1.54, 1.56, and 1.65 nm, respectively. By subtracting the thickness of the calcium niobate perovskite block (1.16 nm),[9a] the average heights of the layered nanospace were 0.38, 0.40, and 0.49 nm, respectively. In contrast, no diffraction peak shift was observed, even at higher loading amount, when the $KCa_2Nb_3O_{10}$ nanosheets were impregnated with the same Pt precursor. In the 5.0 wt% impregnated sample, a small diffraction peak because of metallic Pt was observed, while the adsorption samples did not produce a peak derived from Pt species, even at greater loadings (see Figure S1 in the Supporting Information). These results suggest that the adsorption method provides a high dispersion of Pt into the interlayer nanospace of $KCa_2Nb_3O_{10}$ without forming crystalline Pt aggregates, while the impregnation method does not. In both samples, increasing the loading amount of Pt changed the color of the sample from white to gray, because of the formation of a greater amount of metallic Pt.

XPS measurements were performed to identify the valence state of the deposited Pt species. Figure S2 shows the XPS spectra for Pt 4f in Pt-loaded $KCa_2Nb_3O_{10}$ prepared by adsorption and impregnation, along with reference data for a Pt foil. The spectral shape of the impregnated sample was similar to that of the Pt reference foil, giving two major peaks with binding energies of about 70.0 and 73.5 eV, which were assigned to $4f_{7/2}$ and $4f_{5/2}$ electrons, respectively, of metallic Pt (Pt^0).[18] In addition to the Pt^0 state, two shoulder peaks, assignable to Pt with adsorbed oxygen (Pt-O_{ads}), were observed at binding energies of about 71.5 and 75 eV. However, the Pt 4f spectrum of the adsorption sample differed from those of the impregnation sample and the Pt foil reference. The peak assigned to $4f_{7/2}$ electrons was located at about 72.5 eV, which is a higher binding energy than that of the impregnation sample, but not as high as those of $Pt^{II}O$ species that appear at binding energies of about 73.0–73.5 eV ($4f_{7/2}$ electrons), or that of $[Pt(NH_3)_4]Cl_2$ (73.4 eV).[19] These results indicate that, in the impregnation sample, the loaded Pt species on $KCa_2Nb_3O_{10}$ are almost entirely metallic, while the majority of Pt species in the adsorption sample are in an electron-deficient state suggestive of strong interactions with the oxide nanosheet surface.

The dispersion of Pt nanoparticles in the interlayer nanospaces between the restacked $KCa_2Nb_3O_{10}$ nanosheets was observed by transmission electron microscopy (TEM). The deposited Pt nanoparticles were distinguishable because of the difference in electron density between Pt and the niobate nanosheets. As shown in Figure 2, the adsorption

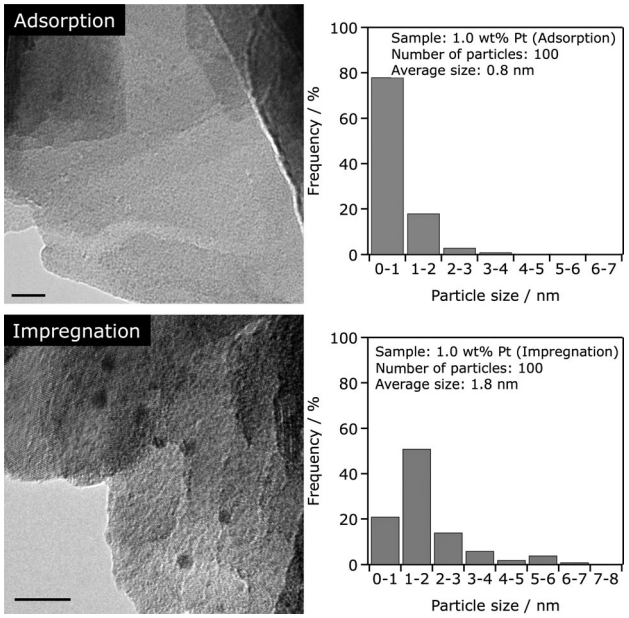

Figure 2. Typical TEM images and corresponding particle size distributions of restacked $KCa_2Nb_3O_{10}$ nanosheets modified with 1.0 wt% Pt using an adsorption and impregnation method (scale bars 10 nm).

sample exhibited very high dispersion of Pt; most of the deposited Pt nanoparticles had a diameter smaller than 1 nm.[20] While some Pt aggregated to form larger secondary particles, the diameter size remained smaller than 4 nm. No deposition of Pt occurred when $H_2[PtCl_6]\cdot 6H_2O$ was used as the precursor in the adsorption method, most likely because of electrostatic repulsion between the anionic Pt complex and polyanion nanosheets. Even at a relatively high loading amount (5.0 wt%), highly dispersed Pt was observed (Figure S3), consistent with the results of the XRD measurements. The impregnated sample (1.0 wt% Pt) also exhibited a high dispersion of Pt deposits with diameters smaller than 3–4 nm, but the average size was greater than that achieved by the adsorption method (Figure 2). When the loading amount was increased to 5.0 wt%, agglomerates with diameters larger than 20 nm were generated (Figure S3), indicating that the Pt species sandwiched by $Ca_2Nb_3O_{10}^-$ nanosheets in the adsorption samples were less susceptible to aggregation upon thermal treatment because of steric hindrance. In addition, the intercalated, highly dispersed Pt nanoclusters underwent interactions with the nanosheet surface, as suggested by XPS (Figure S2), which is favorable for photoredox catalysis, as the efficiency of photocatalytic reactions was improved upon intimate contact between a semiconductor and a co-catalyst.[2b]

Thus, successful intercalation of Pt nanoclusters into the interlayer nanospace of $KCa_2Nb_3O_{10}$ was obtained even at higher Pt loading through simple electrostatic attraction without relying on co-intercalating reagents. According to the same principle, other metal nanoclusters could be introduced into the interlayer nanospaces between $KCa_2Nb_3O_{10}$ nanosheets using the corresponding cationic metal complexes. As shown in Figure S4, highly dispersed metal nanoparticles of Pd, Rh, and Ru were observed, indicating that this methodology could be applicable to various metal species for intercalation.

Unmodified restacked $KCa_2Nb_3O_{10}$ nanosheets exhibited little photocatalytic activity for overall water splitting, producing only a small amount of H_2.[21] As Ebina et al. reported,[10b] $KCa_2Nb_3O_{10}$ with a band gap of about 3.5 eV possessed activity for overall water splitting when modified with RuO_2 (Figure 3), providing confirmation of reproducibility. Platinum-decollated analogs prepared also were active for water splitting. However, the performance of the samples

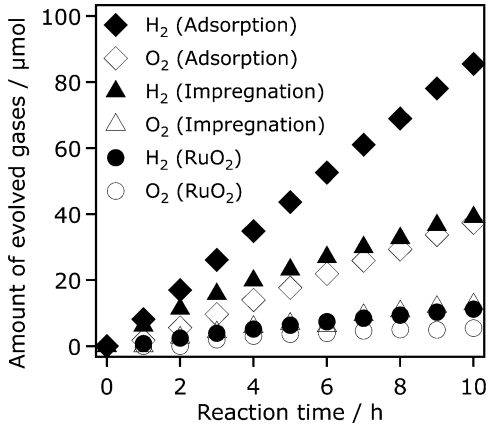

Figure 3. Time course of overall water splitting using $KCa_2Nb_3O_{10}$-based materials under UV irradiation ($\lambda > 300$ nm). Reaction conditions: catalyst, 50 mg; 10 mM aqueous NaI solution, 100 mL; light source, xenon lamp (300 W).

presented here exceeded that of the RuO_2 analog. Results also confirmed that no reaction occurred in the dark or under irradiation of light at wavelengths longer than 380 nm.

The rates of H_2 and O_2 evolution by the adsorption sample were greater than those achieved by an analog with externally decollated Pt, presumably because of the smaller size of the Pt deposits (Figure 2) or the difference in the valence state of Pt, as observed in the XPS spectra (Figure S2). According to a report by Lee and co-workers, an electron-deficient Pt on a semiconductor photocatalyst can act as an electron collector.[22] Therefore, the difference in the Pt valence contributed to the activity difference between the two photocatalysts. The water-splitting rate also was dependent strongly on the amount of Pt loaded. The activity increased with increasing amount of Pt deposition, and reached a maximum at 0.5–1.0 wt%, then decreased (Figure S5). The reproducibility of the rates of H_2 and O_2 evolution in the reaction was within 20% under the same reaction conditions. This adsorption sample exhibited the greatest activity for overall water splitting among nanosheet-based photocatalysts reported.[23]

The stability of Pt-intercalated $KCa_2Nb_3O_{10}$ was tested over 30 h of reaction. As shown in Figure S6, the rates of H_2 and O_2 evolution were improved by a factor of about 1.5 after the first run, then exhibited stable performance without significant loss of activity.[24,25] The total amount of H_2 and O_2 produced in 30 h of reaction was 573 μmol, exceeding that of $Pt/KCa_2Nb_3O_{10}$ (ca. 90 μmol), which clearly confirms the catalytic cycle of the reaction. The apparent quantum yield (AQY) in the steady-state was estimated to be about 3% at 300 nm.[26] Furthermore, no noticeable change in the XRD patterns and XPS spectra for Pt 4f of $Pt/KCa_2Nb_3O_{10}$ before and after the water splitting was identified (Figure S7), indicating that the photocatalyst was stable during water splitting. However, TEM observations showed that the loaded Pt nanoclusters underwent aggregation to some extent after the 30 h of reaction, judging from the change in the histograms (Figure S8).

Recent progress in nanotechnology allowed the examination of the size dependency of metal co-catalysts on activity. Teranishi and co-workers used Rh nanoparticles with a precisely controlled size as a component of core/shell-structured Rh/Cr_2O_3, which is an effective co-catalysts for photocatalytic water splitting.[3d] According to that study, smaller Rh cores exhibited greater activity than the larger Rh cores. In heterogeneous photocatalysis, the effect of co-catalyst size on the photocatalytic water splitting performance had not been examined at sizes smaller than 1 nm because of the lack of an effective preparation method and a suitable photocatalyst. Thus, the results of this study revealed the superior ability of nanoclusters with diameters smaller than 1 nm to promote the water-splitting reaction for the first time.

In summary, the ability of Pt nanoclusters with diameters smaller than 1 nm to promote water-splitting was examined, and a simple method to decollate the interlayer nanospace of a layered metal oxide (here $KCa_2Nb_3O_{10}$) with highly dispersed noble-metal clusters was developed at the same time. The results show the potential of nanosheets as a building block for overall water splitting, which will provide insights for the bottom-up synthesis of photofunctional assemblies based on nanomaterials.

Received: November 27, 2014
Published online: February 5, 2015

Keywords: heterogeneous catalysis · nanosheets · photocatalysis · semiconductors · water splitting

[1] a) B. Dubertret, P. Skourides, D. J. Norris, V. Noireaux, A. H. Brivanlou, A. Libchaber, *Science* **2002**, *298*, 1759 – 1762; b) M. C. Daniel, D. Astruct, *Chem. Rev.* **2004**, *104*, 293 – 346; c) K. K. R. Datta, B. V. S. Reddy, K. Ariga, A. Vinu, *Angew. Chem. Int. Ed.* **2010**, *49*, 5961 – 5965; *Angew. Chem.* **2010**, *122*, 6097 – 6101.

[2] a) W. J. Youngblood, S.-H. A. Lee, K. Maeda, T. E. Mallouk, *Acc. Chem. Res.* **2009**, *42*, 1966 – 1973; b) K. Maeda, *J. Photochem. Photobiol. C* **2011**, *12*, 237 – 268; c) F. E. Osterloh, *Chem. Soc. Rev.* **2013**, *42*, 2294 – 2320.

[3] a) K. Maeda, K. Teramura, D. Lu, N. Saito, Y. Inoue, K. Domen, *Angew. Chem. Int. Ed.* **2006**, *45*, 7806 – 7809; *Angew. Chem.* **2006**, *118*, 7970 – 7973; b) N. Sakamoto, H. Ohtsuka, T. Ikeda, K. Maeda, D. Lu, M. Kanehara, K. Teramura, T. Teranishi, K. Domen, *Nanoscale* **2009**, *1*, 106 – 109; c) K. Maeda, N. Sakamoto, T. Ikeda, H. Ohtsuka, A. Xiong, D. Lu, M. Kanehara, T. Teranishi, K. Domen, *Chem. Eur. J.* **2010**, *16*, 7750 – 7759; d) T. Ikeda, A. Xiong, T. Yoshinaga, K. Maeda, K. Domen, T. Teranishi, *J. Phys. Chem. C* **2013**, *117*, 2467 – 2473.

[4] a) M. Berr, A. Vaneski, A. S. Susha, J. Rodríguez-Fernández, M. Döblinger, F. Jäckel, A. L. Rogach, J. Feldmann, *Appl. Phys. Lett.* **2010**, *97*, 093108; b) E. Khon, K. Lambright, R. S. Khnayzer, P. Moroz, D. Perera, E. Butaeva, S. Lambright, F. N. Castellano, M. Zamkov, *Nano Lett.* **2013**, *13*, 2016 – 2023.

[5] a) M. M. J. Treacy, S. B. Rice, A. J. Jacobson, J. T. Lewandowski, *Chem. Mater.* **1990**, *2*, 279 – 286; b) S. W. Keller, H.-N. Kim, T. E. Mallouk, *J. Am. Chem. Soc.* **1994**, *116*, 8817 – 8818; c) T. Sasaki, M. Watanabe, H. Hashizume, H. Yamada, H. Nakazawa, *J. Am. Chem. Soc.* **1996**, *118*, 8329 – 8335.

[6] A. Lopez-Galindo, C. Viseras, P. Cerezo, *Appl. Clay Sci.* **2007**, *36*, 51 – 63.

[7] a) W. Sugimoto, H. Iwata, Y. Yasunaga, Y. Murakami, Y. Takasu, *Angew. Chem. Int. Ed.* **2003**, *42*, 4092 – 4096; *Angew. Chem.* **2003**, *115*, 4226 – 4230; b) H. Zheng, F. Tand, Y. Jia, L. Wang, Y. Chen, M. Lim, L. Zhang, G. Lu, *Carbon* **2009**, *47*, 1534 – 1542; c) M. Osada, T. Sasaki, *Adv. Mater.* **2012**, *24*, 210 – 228.

[8] a) A. Takagaki, M. Sugisawa, D. Lu, J. N. Kondo, M. Hara, K. Domen, S. Hayashi, *J. Am. Chem. Soc.* **2003**, *125*, 5479 – 5485; b) A. Takagaki, D. Lu, J. N. Kondo, M. Hara, S. Hayashi, K. Domen, *Chem. Mater.* **2005**, *17*, 2487 – 2489; c) C. Tagusagawa, A. Takagaki, S. Hayashi, K. Domen, *J. Am. Chem. Soc.* **2008**, *130*, 7230 – 7231.

[9] a) Y. Ebina, A. Tanaka, J. N. Kondo, K. Domen, *Chem. Mater.* **1996**, *8*, 2534 – 2538; b) R. Abe, K. Shinohara, A. Tanaka, M. Hara, J. N. Kondo, K. Domen, *Chem. Mater.* **1997**, *9*, 2179 – 2184.

[10] a) Y. Ebina, T. Sasaki, M. Harada, M. Watanabe, *Chem. Mater.* **2002**, *14*, 4390 – 4395; b) Y. Ebina, N. Sakai, T. Sasaki, *J. Phys. Chem. B* **2005**, *109*, 17212 – 17216; c) Y. Ebina, K. Akatsuka, K. Fukuda, T. Sasaki, *Chem. Mater.* **2012**, *24*, 4201 – 4208.

[11] a) S.-M. Paek, H. Jung, Y.-J. Lee, M. Park, S.-J. Hwang, J.-H. Choy, *Chem. Mater.* **2006**, *18*, 1134 – 1140; b) T. W. Kim, S. G. Hur, S.-J. Hwang, H. Park, W. Choi, J.-H. Choy, *Adv. Funct. Mater.* **2007**, *17*, 307 – 314; c) J. L. Gunjakar, T. W. Kim, H. N. Kim, I. Y. Kim, S.-J. Hwang, *J. Am. Chem. Soc.* **2011**, *133*, 14998 – 15007.

[12] a) O. C. Compton, E. C. Carroll, J. Y. Kim, D. S. Larsen, F. E. Osterloh, *J. Phys. Chem. C* **2007**, *111*, 14589 – 14592; b) M. R. Allen, A. Thibert, E. M. Sabio, N. D. Browning, D. S. Larsen, F. E. Osterloh, *Chem. Mater.* **2010**, *22*, 1220 – 1228; c) E. M. Sabio, R. L. Chamousis, N. D. Browning, F. E. Osterloh, *J. Phys. Chem. C* **2012**, *116*, 3161 – 3170.

[13] a) H. Hata, Y. Kobayashi, V. Bojan, W. J. Youngblood, T. E. Mallouk, *Nano Lett.* **2008**, *8*, 794 – 799; b) R. Ma, Y. Kobayashi, W. J. Youngblood, T. E. Mallouk, *J. Mater. Chem.* **2008**, *18*, 5982 – 5985.

[14] a) K. Maeda, M. Eguchi, W. J. Youngblood, T. E. Mallouk, *Chem. Mater.* **2008**, *20*, 6770 – 6778; b) K. Maeda, M. Eguchi, S.-H. A. Lee, W. J. Youngblood, H. Hata, T. E. Mallouk, *J. Phys. Chem. C* **2009**, *113*, 7962 – 7969; c) K. Maeda, M. Eguchi, W. J. Youngblood, T. E. Mallouk, *Chem. Mater.* **2009**, *21*, 3611 – 3617; d) K. Maeda, T. E. Mallouk, *J. Mater. Chem.* **2009**, *19*, 4813 – 4818; e) T. Oshima, O. Ishitani, K. Maeda, *Adv. Mater. Interfaces* **2014**, *1*, 1400131; f) K. Maeda, M. Eguchi, T. Oshima, *Angew. Chem. Int. Ed.* **2014**, *53*, 13164 – 13168; *Angew. Chem.* **2014**, *126*, 13380 – 13384.

[15] a) Y. Okamoto, S. Ida, J. Hyodo, H. Hagiwara, T. Ishihara, *J. Am. Chem. Soc.* **2011**, *133*, 18034 – 18037; b) S. Ida, Y. Okamoto, M. Matsuka, H. Hagiwara, T. Ishihara, *J. Am. Chem. Soc.* **2012**, *134*, 15773 – 15782; c) S. Ida, A. Takashiba, S. Koga, H. Hagiwara, T. Ishihara, *J. Am. Chem. Soc.* **2014**, *136*, 1872 – 1878.

[16] a) A. Kudo, A. Tanaka, K. Domen, K. Maruya, K. Aika, T. Onishi, *J. Catal.* **1988**, *111*, 67 – 76; b) A. Kudo, K. Sayama, A. Tanaka, K. Asakura, K. Domen, K. Maruya, T. Onishi, *J. Catal.* **1989**, *120*, 337 – 352.

[17] a) H. Hata, S. Kubo, Y. Kobayashi, T. E. Mallouk, *J. Am. Chem. Soc.* **2007**, *129*, 3064 – 3065; b) H. Hata, Y. Kobayashi, M. Salama, R. Malek, T. E. Mallouk, *Chem. Mater.* **2007**, *19*, 6588 – 6596.

[18] K. S. Kim, N. Winograd, R. E. Davis, *J. Am. Chem. Soc.* **1971**, *93*, 6296 – 6297.

[19] Y. V. Salyn, V. I. Nefedov, A. G. Makarova, G. N. Kuznetsova, *Zh. Neorg. Khim.* **1978**, *23*, 829.

[20] The size of intercalated Pt nanoclusters estimated from TEM observations (ca. 1 nm) was larger than the height of the interlayer distance calculated from XRD peak positions (0.40 nm). This contradiction can be explained as follows. Because the nanosheet is structurally flexible, expansion of interlayer would occur near the sites where Pt nanoclusters are deposited, while the unloaded region would not contribute to the expansion. Of course, XRD data give us "average" information on a given material. In this specific case, namely, we observed the average interlayer distance of the expanded and unexpanded regions. This could explain the inconsistency between the calculated interlayer distance by XRD and the mean size of the Pt nanoparticles determined by TEM observations.

[21] The water-splitting reactions were conducted in pure water containing 10 mM NaI to minimize the undesirable H_2/O_2 recombination that occurs on Pt during the reaction according to the report by Abe et al. (*Chem. Phys. Lett.* **2003**, *371*, 360–364.). The details are included in the Supporting Information.

[22] J. S. Jang, S. H. Choi, H. G. Kim, J. S. Lee, *J. Phys. Chem. C* **2008**, *112*, 17200 – 17205.

[23] The performance of $Pt/KCa_2Nb_3O_{10}$ is obviously much higher than that of RuO_2-loaded $KCa_2NaNb_4O_{13}$, which has been recently reported by Ebina et al. (Ref. [10c]), because $RuO_2/KCa_2NaNb_4O_{13}$ shows only an about 1.3 times higher activity than $RuO_2/KCa_2Nb_3O_{10}$ (see Refs. [10b and c]).

[24] It was shown by means of ion chromatography that I^- ions in the reactant solution did not undergo oxidation by the valence band holes in $Pt/KCa_2Nb_3O_{10}$ during the water-splitting reaction, even though they are more susceptible to oxidation than water. In other words, water oxidation occurred efficiently on the surface of restacked $KCa_2Nb_3O_{10}$ nanosheets. This is consistent with our recent study (Ref. [14e]).

[25] The activity was improved by about 1.5 times after the first run. Almost identical phenomenon has been observed in other photocatalytic overall water splitting systems using Pt-loaded semiconductor in an aqueous NaI or KI solution (for example, Pt/TiO_2: R. Abe et al., *Chem. Phys. Lett.* **2003**, *371*, 360 – 364; Coumarin dye/$Pt/H_4Nb_6O_{17}$: R. Abe et al., *J. Am. Chem. Soc.* **2013**, *135*, 16872 – 16884), but not in pure water. Therefore, this appears to be a characteristic feature in the iodide ion-based overall water splitting system, although the reason has not been clarified yet.

[26] We tried to measure AQY of the reaction with monochromatized light. Due to the occurrence of undesirable reverse reaction of water formation from H_2 and O_2 that still occurred even in an aqueous NaI solution, however, we did not obtain measurable gas product. Therefore, we compared the O_2 evolution rate in overall water splitting recorded in the present study to that achieved by $RuO_2/KCa_2Nb_3O_{10}$ in an aqueous $NaIO_3$ solution (Ref. [14e]).

